Ocean Modelling 40 (2011) 190–198

Contents lists available at SciVerse ScienceDirect

Ocean Modelling

journal homepage: www.elsevier.com/locate/ocemod

Nesting a nonhydrostatic model in a hydrostatic model: The boundary interface

P.C. Gallacher [a,*], D.A. Hebert [a], M.R. Schaferkotter [b]

[a] Naval Research Laboratory, Ocean Sciences Division, Stennis Space, MS 39529, USA
[b] Jacobs Technology Inc., 1020 Titan Court, Fort Walton Beach, FL 32547, USA

ARTICLE INFO

Article history:
Received 2 February 2011
Received in revised form 11 August 2011
Accepted 15 August 2011
Available online 2 September 2011

Keywords:
Nonhydrostatic model
Boundary conditions
Nested models
Prediction
Internal waves
Nonlinear waves

ABSTRACT

A method is developed for adjusting the values of the prognostic variables near the interface between a nonhydrostatic, high resolution model embedded in a hydrostatic, coarser resolution model. It incorporates a method of conditioning the outer domain lateral boundary values to enforce conservation of volume when the variables are interpolated onto the inner domain grid. This is accomplished by adjusting the baroclinic normal velocities at the open boundaries after interpolation. The method also includes a relaxation scheme which matches the values of the prognostic variables across a narrow zone near the open boundaries of the submesoscale inner domain. This prevents the development of discontinuities, reflections and perimeter currents at the periphery of the inner domain. Submesoscale hindcasts are conducted in areas of high Nonlinear Internal Wave (NLIW) activity. Since NLIWs have amplitudes, O(100 m), which are not small relative to their wavelengths, O(100 – 1000 m) these hindcasts require a nonhydrostatic model in the inner domain. Since the hydrostatic model lacks the physics and resolution to support NLIWs there will be discrepancies between the values of the hydrostatic and nonhydrostatic prognostic variables at the boundaries. It is shown that the application of these method for adjusting the values of the prognostic variables near the interface allows the computation of a nonhydrostatic, submesoscale hindcast forced by a nested hydrostatic forecasting system.

Published by Elsevier Ltd.

1. Introduction

Modeling submesoscale dynamics, scales of O(10 m–1 km), requires resolutions that preclude global modeling and dynamics that are unnecessary for global scales. In order to model submesoscale dynamics as part of a global forecasting system, as is the ultimate goal, a smaller model domain with open boundaries derived from a coarser, larger scale model is required. Thus, some method(s) must be employed to handle the open boundaries of the submesoscale domain. As the name open boundary implies fluid must be able to flow freely in and out of the model domain. Also scales of motion too large to be contained in the submesoscale domain must correctly influence the flow in the domain. The boundaries of the submesoscale domain should be truly transparent, i.e. they should be invisible in the results of the modeling.

In this paper we focus on the requirements for the open boundary conditions between a submesoscale, nonhydrostatic inner domain and a mesoscale, hydrostatic outer domain for a one-way coupled case. The submesoscale resolution allows dynamic features to be resolved which are not captured at mesoscale resolution. Furthermore, in order to model submesoscale dynamics which includes Nonlinear Internal Waves (NLIWs) with large amplitude (hundreds of meters) and subinertial eddies and filaments a nonhydrostatic model with resolution of tens to hundreds of meters in the horizontal and meters to tens of meters in the vertical is required. The difference in the physics between the nonhydrostatic model and the hydrostatic model will also lead to differences in the solutions that exacerbate the problems of interfacing the nested models. When a mismatch of the solutions occurs at the interface between the domains spurious reflections and erroneous perimeter currents along the boundaries (Mason et al., 2010) can result. Also incorrect geostrophic currents can be set up along the open boundaries by erroneous density gradients across the boundaries.

The open boundary conditions (OBCs) must be effective at providing information to the inner domain from the outer domain and at propagating information out of the inner domain. Both requirements must be accomplished transparently. In one-way coupling, which is the focus of this paper, the information propagated out of the inner domain does not affect the outer domain. Because of the differences in physics and resolution there will be inherent differences between the mesoscale solution and the submesoscale solution. Prognostic variables from the coarse grid must be interpolated onto the fine grid in a manner that conserves basic properties and scales. This interpolation can be problematic since the most common interpolation schemes are not conservative, e.g. bilinear and nearest neighbor (Guo et al., 2003 and Accadia et al., 2003).

* Corresponding author. Address: Naval Research Laboratory, Ocean Sciences Division, Code 7331, Bldg 1009, Stennis Space Center, MS 39529, USA. Tel.: +1 228 688 5315; fax: +1 228 688 5997.
E-mail address: Patrick.Gallacher@nrlssc.navy.mil (P.C. Gallacher).

1463-5003/$ - see front matter Published by Elsevier Ltd.
doi:10.1016/j.ocemod.2011.08.006

Formulating and applying OBCs to limited area models is challenging and complex. This has been an active area of research for some time, see reviews by Palma and Matano (1998) and Davies (1983). OBC methods can be divided into two categories: (1) adaptive and (2) consistent. Adaptive methods differentiate between incoming and outgoing fluxes and apply different OBCs values based on the direction of the flux. Consistent OBCs apply the same value regardless of the direction of the boundary flux.

The advantage of using adaptive OBCs is that different OBCs can be applied for each case. This allows the response to be tailored to the characteristics and scales of the outer domain or inner domain solution as appropriate (Marchesiello, 2001). Disadvantages of adaptive OBCs include: determining which points qualify as inflow and which qualify as outflow, handling transitions between adjacent inflow and outflow areas and handling strong tangential flows. Adaptive OBCs are further complicated by the fact that any open boundary point could simultaneously be an inflow point for some scales and an outflow point for others.

On the other hand, consistent OBCs apply the same method to all open boundary points. These methods are typically a form of wave radiation, absorption or relaxation scheme. Problems with radiation schemes stem from the fact that multiple waves with different phase speeds will exist in realistic cases; whereas the radiation schemes use only one phase speed. Absorption schemes typically have a region where the viscosity is artificially increased to damp the solution near the boundaries. Relaxation schemes involve a region near the boundaries in which the inner and outer values are smoothly merged. One issue with relaxation and absorbing layers is that the equations governing the motion in the boundary layer are not the correct equations for any approximation of the physics so spurious solutions can result. See Blayo and Debreu (2005) for a discussion of OBCs based on characteristics. In this paper we focus on methods for consistent OBCs and the particulars of the methods are discussed below.

For simulations involving idealized or climatological case studies of processes the large scale flow can be prescribed as constant or a simple function of time and the OBCs merge these values with the flow field from the submesoscale domain. For predictions whether in real-time, i.e. forecasts, or offline, i.e. hindcasts, the problem is more complicated. In these cases the OBCs must be able to merge the multiple time and space scales of the larger scale dynamics and the multiple time and space scales of the resolved submesoscale dynamics.

The remainder of this paper is divided as follows: Section 2 which discusses the boundary conditioning methods we have employed, Section 3 which describes the model and the domain for the experiments, Section 4 which describes the results of several experiments demonstrating these boundary conditioning methods, and Section 5 which summarizes the results and gives some conclusions.

2. Boundary conditioning

We have extended and improved two OBC methods which together correct the problems of conservation and matching at the interface between a hydrostatic outer domain and a nonhydrostatic inner domain. The first method is the Transport Correction Scheme (TCS). OBCs are formulated to conserve volume by matching the change in sea surface elevation, η, and the total transport through the lateral boundaries and distributing the difference into the baroclinic transports. The second method is the Flow Relaxation Scheme (FRS). In the Flow Relaxation Scheme OBCs are constructed to prevent reflections and perimeter currents which can be generated when flows do not exit the interior domain correctly. This is related to a mismatch of coarse and fine resolution values near the interface. The FRS allows outer domain values to propagate into the inner domain with minimal distortion.

2.1. Transport Correction Scheme

The outer domain values are interpolated to the inner domain grid at points along the lateral boundaries using bilinear interpolation. η is also interpolated from the coarse grid to the fine grid. Additionally since the outer domain is a part of an operational system the values may have been interpolated onto different grids for archiving or analysis purposes prior to the interpolation onto the inner domain grid. Each interpolation can generate errors resulting in a loss of volume conservation. For both the transport and η, and particularly the former, the interpolation is not conservative (Guo et al., 2003). Furthermore, the fact that the transport and η are interpolated separately can lead to an imbalance between the fields (Shulman et al., 2002). Small errors in the normal velocities through the sides can cause significant changes in transport into the inner domain and this is reflected in large deviations in η over time.

Volume conservation requires that the net transport through the lateral boundaries is equal to the temporal change of η in the inner domain. However, the geometry of ocean domains, i.e. small aspect ratio (h/L) guarantees that the change in η will be small. Therefore, we correct the transport through the domain by setting the average transport to zero for every time interval between the outer domain boundary values (one hour in this case).

The average transport through the lateral boundaries can be specified as:

$$\varsigma_{\tau_1} = \frac{1}{\tau_2 - \tau_1} \int_{\tau_1}^{\tau_2} \oint_{\Gamma} \int_0^h u_n(b,z) dz\, h(b) db\, dt \tag{1}$$

where b are the points along the open boundary, Γ, u_n is the normal baroclinic velocity at b, h is the depth at b and τ_1 and τ_2 are successive outer domain data time points. The change in η averaged over the inner domain is given by

$$\bar{\eta}_t = \frac{\partial}{\partial t} \frac{\iint_S \eta dS}{\iint_S dS} \tag{2}$$

where S is the surface area of the inner domain. If volume is conserved then $\zeta_{\tau_1} = \overline{\eta}_t$. However, as we have discussed above interpolation and other factors prevent this equality from holding. Thus we have

$$\varsigma_{\tau_1} = \bar{\eta}_t + \varepsilon_\zeta \approx \varepsilon_\zeta \tag{3}$$

where ε_ζ is the error in the transport and it is much larger than $\overline{\eta}_t$. This imbalance is corrected by adjusting u_n uniformly at every grid point along the open boundaries at every inner domain timestep based ε_ζ. Thus

$$u_n^*(b,z) = u_n(b,z) - \frac{\varepsilon_\zeta}{\oint_\Gamma h(b) db} \cdot \hat{n} \tag{4}$$

is the corrected baroclinic normal velocity from the outer domain interpolated onto the open boundary of the inner domain where $\hat{n}$ is the inward directed normal vector at the boundary.

2.2. Flow Relaxation Scheme

Differences in resolution, physics, and numerics will cause hydrodynamic features to be different in scale and dynamics between the outer and inner domains. No errors that arise due to variations between these values can be allowed to propagate into the inner domain. To accomplish this a relaxation zone is included in the inner domain adjacent to the lateral boundaries. The relaxation

zone is an area where the fluxes of conserved baroclinic quantities from the coarse and the fine grids are matched.

Relaxing the solutions can be viewed as two separate problems. First allowing outwardly directed fluxes to exit smoothly and without reflection or the generation of artificial perimeter currents. Second allowing the fluxes from the outer domain to enter and affect the inner solution without creating a discontinuity or being excessively damped. Each problem is addressed below.

The first problem has been addressed by radiation or diffusion of conserved quantities. Radiation OBCs such as Flather et al. (1976), or Orlanski (1976) assume that a wave, usually barotropic, propagates the conserved quantities out of the inner domain. The problem with Flather and Orlanski OBCs is that there is only one phase speed so multiple waves and non-wave phenomena, such as eddies and filaments are not propagated out of the domain effectively. Nevertheless the Flather OBC has had some success in realistic three dimensional hydrostatic models. In fact the Flather boundary condition insures near conservation for mass and energy through the open boundary (Blayo and Debreu, 2005). For example, it is used when nesting Navy Coastal Ocean Model (NCOM) domains and is sufficient to maintain volume conservation in the inner domain (C. Rowley, personal communication) without explicitly enforcing conservation of baroclinic values at the lateral boundaries. However, this did not work for the nonhydrostatic submesoscale domain we are implementing. Thus we had to construct a new set of OBCs.

Diffusive techniques employ a form of sponge or absorbing layer where the viscosity and diffusivity are artificially increased, damping the inner domain conserved quantities to zero as the boundary is approached. The damping needs to be smooth and complete such that there is no reflection back into the domain and no generation of spurious modes in the relaxation zone.

The second problem requires a technique for matching the solutions across the boundary. A method to accomplish this is the Flow Relaxation Scheme (FRS). Several schemes were reviewed by Davies (1983) and were further described by Martinsen and Engedahl (1987). The FRS method was expanded by Lavelle and Thacker (2008), hereafter referred to as LT08. Various geometric forms for the relaxation coefficient have been proposed by Jensen (1998) and Modave et al. (2010) (hereafter referred to as MDD10). All of these formulations were for barotropic OBCs, here we apply the method to the baroclinic OBCs.

The basic formulation for the FRS is

$$\frac{D\chi}{Dt} = RHS - \sigma(n)\chi \tag{5}$$

where χ is any of the baroclinic prognostic variable, e.g. temperature, T, salinity, S, eastward velocity, u, or northward velocity, v. RHS represents all the terms on the right hand side of the Eulerian equation describing the total rate of change, D/Dt, of the prognostic variable χ and $\sigma(n)$ is the relaxation coefficient in the relaxation zone. Note that the relaxation zone is part of the inner domain solution with the addition of the relaxation term. In the relaxation zone the coordinate normal to the boundary is n. The width of the relaxation zone is $\delta = N\Delta n$ with $n = 0$ at the interior edge of the relaxation zone (Fig. 1). Note that σ can also be a function of the tangential coordinate in the relaxation zone as in the "simple" relaxation scheme of LT08. However, as noted by LT08, variation of σ tangentially is only necessary in the case of poorly defined outer domain values. In our case those values are well defined since we are using a nested model solution rather than climatology.

MDD10 defines a characteristic length scale for the damping of features, i.e. the width of the relaxation zone, in terms of a barotropic gravity wave speed and the damping coefficient as

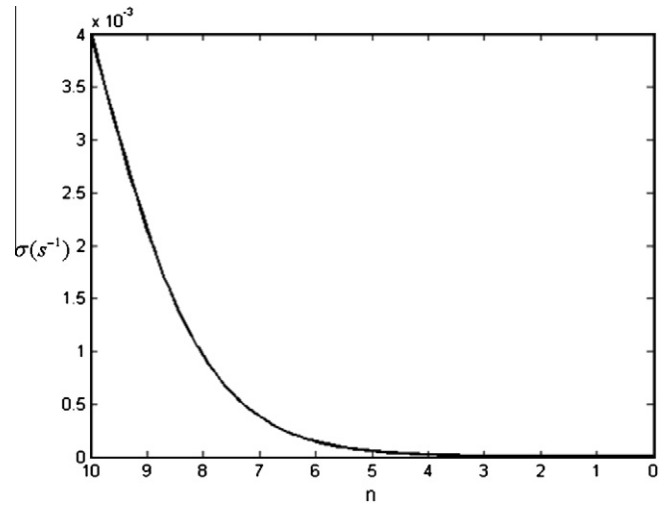

Fig. 1. Schematic of the relaxation zone at western boundary showing value of $\sigma(n)$ where n is the coordinate normal to the boundary and width of relaxation zone ($\delta = N\Delta n$, $N = 10$) gridpoints). Similar relaxation zones exist inside each of the four lateral boundaries between the inner domain and the outer domain.

$$\delta = \frac{\sqrt{gh}}{\sigma} \tag{6}$$

We generalize (6) to

$$\delta = \frac{u_n}{\sigma} \tag{7}$$

where u_n is the nominal normal velocity of the dominant baroclinic feature moving through the relaxation zone. If l_n is the nominal length scale of the features to be modified in the relaxation zone, then the width of the relaxation zone should be approximately $\delta = N\Delta n > l_n$ where N is order 10. Then we suggest that the optimal absorption coefficient scales like

$$\sigma \approx \frac{u_n}{N\Delta n} \tag{8}$$

MDD10 and several other authors argue that the relaxation zone is more effective if σ varies spatially across the relaxation zone. MDD10 compares several geometric forms for σ including a polynomial form

$$\sigma(n) = \sigma_m \left(\frac{n}{\delta}\right)^{\alpha} \tag{9}$$

where $\alpha > 0$ and σ_m is the value at the outer edge of the relaxation zone. When $\alpha = 2$ this reduces to the quadratic form of LT08 for their "simple" sponge layer. We tested that form and a hyperbolic tangent form,

$$\sigma(n) = \sigma_m \tanh\left(\frac{n}{\delta}\right), \tag{10}$$

which was suggested by Martinsen and Engedahl (1987) and Jensen (1998). We found that the hyperbolic tangent worked best.

Based on the above discussion and some experimentation the relaxation zone in our model is 10 grid points wide. The optimal value of σ_m is 0.004 for our case based on tests described below. The spatial variation of σ is given by (10) (see Fig. 1, which also shows the grid convention in the relaxation zone). There is a relaxation zone adjacent to each of the four boundaries.

3. Models and domains

The nested configuration (Fig. 2) used for these experiments consists of an inner domain using the MIT model in a 2°E × 1°N

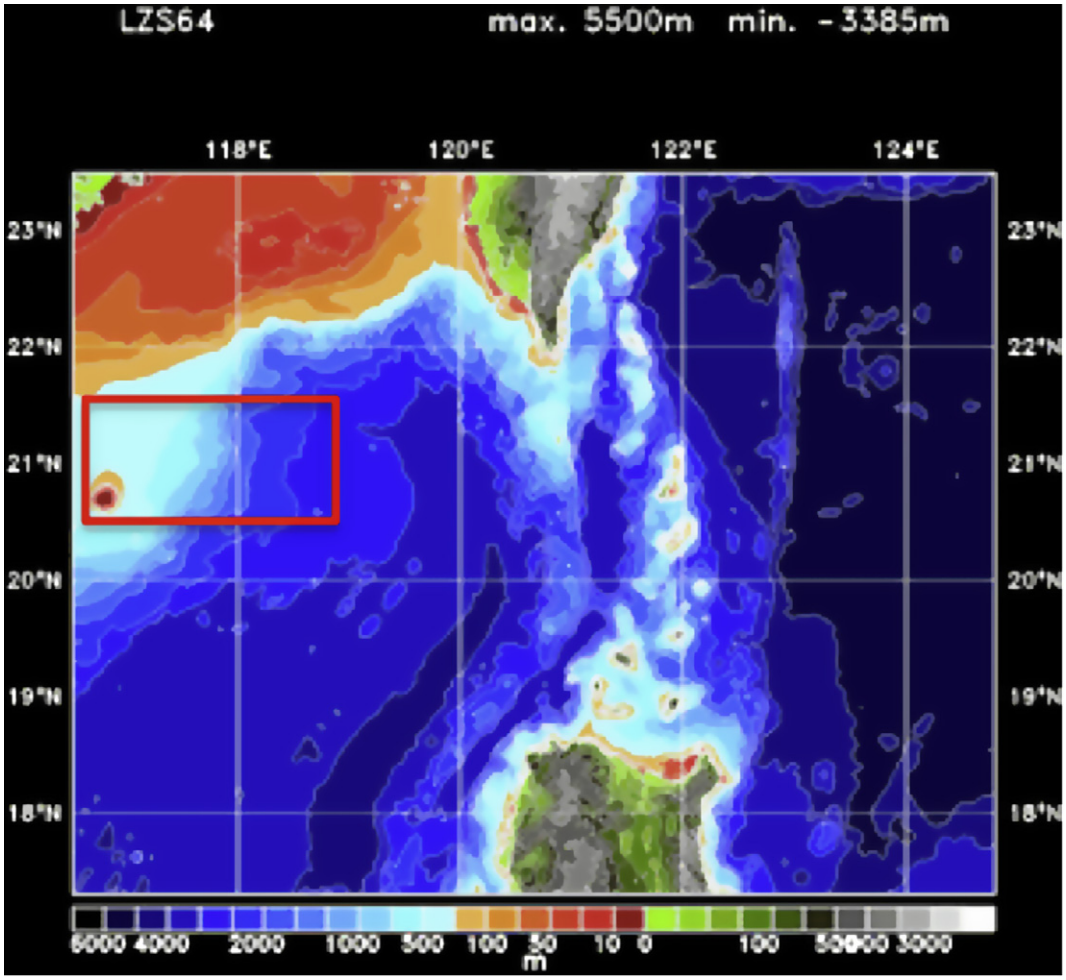

Fig. 2. Luzon Straits 1/64° (LZS64) RELO NCOM domain with the Dongsha Plateau 1/200° (DSP200) MIT domain shown by the red rectangle (Dongsha Island is the red dot in the southwestern corner of the DSP200 domain).

domain centered at (21°N, 117.75°E) with 1/200° (approximately 500 m) horizontal resolution which we name the DSP200 (Dongsha Plateau 1/200°) domain. This is nested inside an outer domain using a 8°E × 6°N RELO NCOM (Coelho et al., 2009) domain at 1/64° (approximately 2 km) horizontal resolution which is named the LZS64 (Luzon Straits 1/64°) domain (Chao et al., 2007). The LZS64 domain obtains its initial conditions and boundary conditions from archived data. The data was archived during forecasts by a 59°E × 45°N regional NCOM domain at 1/16° (approximately 6–9.5 km) resolution designated the EAS16NFS (East Asian Seas 1/16° Nowcast/Forecast System) (Riedlinger et al., 2006). The EAS16NFS is part of the 1/8° (nominally 14 km resolution) Global NCOM Nowcast/Forecast system (Barron et al., 2006).

Table 1
Model parameters.

	Latitude (x)	Longitude (y)	z
Nominal grid spacing	1/200° (500 m)	1/200° (500 m)	0.75–270 m
Number of grid points	348	200	35
Viscosity (m^2s^{-1})	0.24	0.24	7.0×10^{-4}
Temperature diffusivity (m^2s^{-1})	3.4	3.4	1.0×10^{-4}
Salinity diffusivity (m^2s^{-1})	3.4×10^{-2}	$3.4x10^{-2}$	1.0×10^{-6}
Time step (s)	5		

The MITgcm nonhydrostatic ocean model (Marshall et al., 1997a, b) is an open source code which is available to the community, (http://mitgcm.org/). It is a finite volume model with orthogonal curvilinear coordinates in the horizontal and variable cell thickness in the vertical. Several options are available for advection and diffusion calculations. In nonhydrostatic mode a three dimensional equation must be solved for the pressure. This is done using a preconditioned conjugate gradient solver. The model includes a complete treatment of the Coriolis force and a partial cell treatment of topography (Adcroft et al., 1997). The model uses a flexible domain decomposition method for efficient parallel processing, allowing it to be run on modern supercomputers. The model parameters for this study are given in Table 1.

The global NCOM nowcast/forecast system is forced with the Navy Operational Global Atmospheric Prediction System (NOGAPS) (Hogan and Rosmond, 1991) and with a regional forecast system, the Coupled Ocean Atmosphere Prediction System (COAMPS) (Hodur, 1997). Also equilibrium tides are obtained from the OSU (Egbert et al., 1994) global tidal database. Ten constituents are included: K1, O1, P1, Q1, M2, S2, N2, K2, MF, MM. This includes both height and velocity values of the tides. The bathymetry used for the system is the 2 min NRL Digital Bathymetric DataBase (NRL DBDB2, http://www7320.nrlssc.navy.mil/DBDB2_WWW/), a global 2-min ocean bathymetry data base which is based on the NAVO global 5-min DBDBV bathymetry and is enhanced with other higher resolution bathymetries and coastlines. The model also

assimilates satellite altimeter data and Multi-Channel Sea Surface Temperature (MCSST) from satellite-derived AVHRR to further improve accuracy.

4. Results

Submesoscale, nonhydrostatic hindcasts were conducted in the DSP200 domain for 30 days starting on April 1, 2005 at 0000Z. The hindcasts were initialized using archived data from LZS64 and the boundary conditions were also from LZS64 data archived at one hour intervals. The initial data included baroclinic tides, long wavelength internal waves and fronts that develop into NLIWs in the nonhydrostatic domain.

4.1. Transport Correction Scheme

Initially we coupled the domains using a Flather boundary condition on the barotropic flow and no explicit conservation scheme for the baroclinic flow field. This is a standard practice in coupled ocean models and conserves mass sufficiently for most cases (Blayo and Debreu, 2005) and (C. Rowley, personal communication). However, in our case this produced significant phase errors in η which caused us to examine the sea surface elevation variations in more detail. The change in spatial mean sea surface elevation in the inner domain, $\overline{\eta_t^D}$, which results from the transport based on (1) is

$$\overline{\eta_t^D} = \varsigma_{\tau_1} \tag{11}$$

The values of $\overline{\eta_t^D}$, which decrease to a minimum of 30 m and then increase to a maximum of nearly 18 m, are unrealistically large and indicate erroneously large changes in volume. This is typical of boundary conditions with non-conservative transport as discussed in Section 2 above.

The TCS described in Section 2.1 was applied to the normal velocities interpolated from the outer domain at the lateral boundaries of the inner domain. The resulting $\int_\tau \overline{\eta_t^D} dt$ is shown in Fig. 3. The values are much smaller than the uncorrected values indicating that the corrected transport achieves a much better approximation of volume conservation. Large oscillations or large trends in $\overline{\eta_t^D}$ can be viewed as an indicator of the error in the volume transport which resulted from the interpolation of the outer domain variables onto the inner domain grid. As $\overline{\eta_t^D}$ becomes smaller it exhibits more realistic values and temporal variability such as the tidal variations, which can be seen in Fig. 3.

Without the TCS the values of $\overline{\eta_t^D}$ were -30 m to 20 m. With the TCS we obtain values for $\overline{\eta_t^D}$ of 0.6 to 1.4 m. Point measurements of η in the northern South China Sea yield values of 0.3 m to 0.7 m (Beardsley et al., 2004) and (Lien et al., 2005) and tidal models give 0.6–1.0 m (Jan et al., 2007). The values of $\overline{\eta_t^D}$ may still be slightly large; however, the they are in much better agreement with point observations than before. The TCS also reduces erroneous trends in thermocline displacement and volume averaged temperature in the model results.

4.2. Flow Relaxation Scheme

Ideally the open boundaries of a nested model should be transparent to both incoming and outgoing flows. However, some submesoscale features, e.g. eddies and NLIWs are sometimes reflected at the open boundaries where they should propagate out of the inner domain (Fig. 4, top row). This is due to the mismatch of properties, such as propagation speed and amplitude, between the inner domain representation of the features and the outer domain representation of the features. The increased resolution in the inner domain allows features to develop with smaller scales, larger amplitudes and different phase speeds than the outer domain representation of the same features. Also features will develop that are not resolved in the outer domain. This is due to improved dynamical resolution and lower numerical viscosity. Furthermore, the nonhydrostatic physics includes a more complete representation of the vertical momentum resulting in more robust vertical motion in the inner domain and additional features.

In addition to reflections, mismatches between the inner domain and outer domain solutions can cause the formation of currents flowing along the perimeter of the inner domain. We find some evidence of perimeter currents in our numerical experiments usually associated with reflections. However, the reflections are more abundant and much more disruptive. Also we find that eliminating the reflections also eliminates the perimeter currents so we focus on eliminating reflections from the boundaries.

The FRS discussed in Section 2 was employed to reduce or eliminate these problems. The FRS matches the outer domain solution and the inner domain solution in a relaxation zone adjacent to the interface between the domains (Fig. 1). Experiments designed to determine the optimal FRS were compared graphically and using

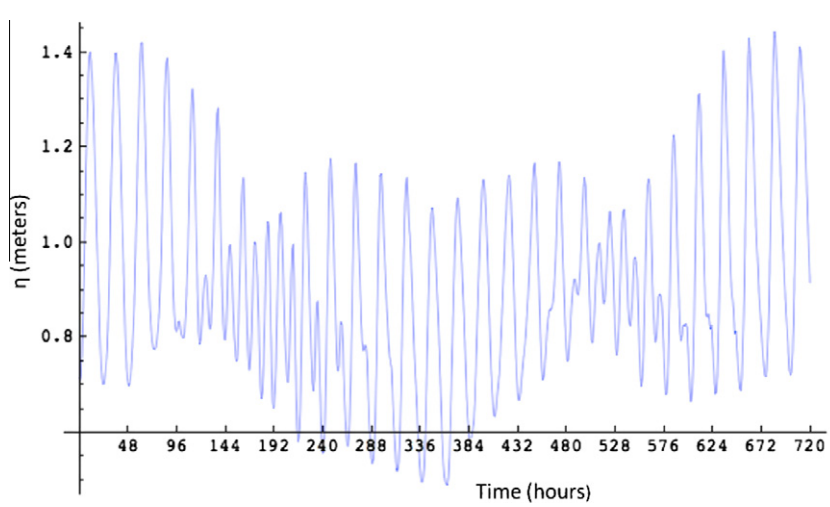

Fig. 3. Average sea surface height, $\overline{\eta}$, after application of the Transport Correction Scheme (TCS). The smaller range of $\overline{\eta}$ indicates improved volume conservation. The tidal signal, which is a strong component of the forcing in this area, is now clearly visible.

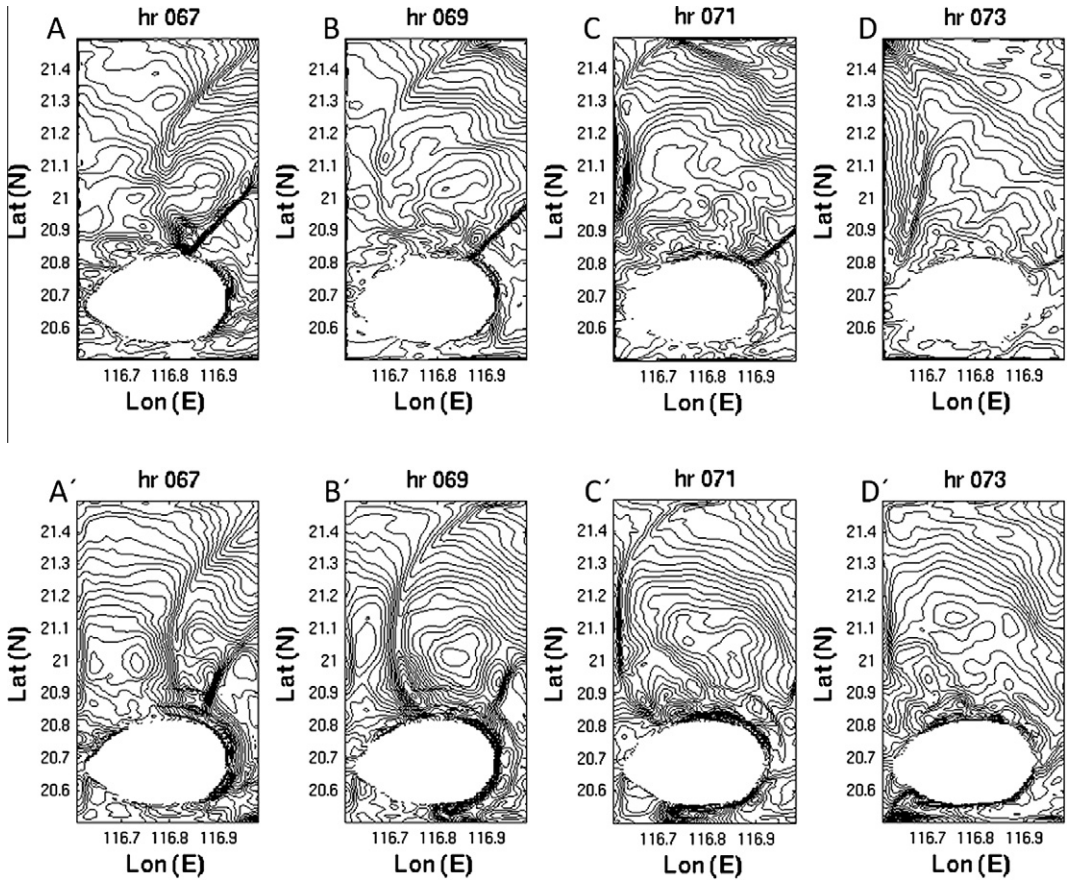

Fig. 4. Temperature at 150 m. Top row is the experiment with no FRS. Bottom row is the FRS experiment. In panels A and A′ a NLIW is clearly visible in the middle of the panel. In B and B′ the waves propagate toward the western boundary. In C and C′ the waves arrive at the western boundary. In D the wave has reflected into the domain. In D′ there is no reflected wave.

the total kinetic energy averaged over the inner domain for the entire experiment,

$$\overline{\overline{KE}} = \frac{1}{T}\int \frac{1}{V}\iiint_V (u^2 + v^2 + w^2)dVdt \tag{12}$$

as a quantitative metric. $\overline{\overline{KE}}$ is chosen as a metric because waves artificially reflected from the boundaries will increase the $\overline{\overline{KE}}$ in the inner domain. This is explored further below.

The reflection of NLIWs at the lateral boundaries of the inner domain can be seen most clearly at the western boundary. The hydrostatic representation of the NLIWs generally enter the inner domain through the eastern boundary. They are transformed by the nonhydrostatic physics and improved resolution in the inner domain and by interactions with the topography. More NLIWs are locally generated and these interact with the remotely generated NLIWs as they propagate across the inner domain in a mainly westerly direction. Thus the mismatches between the low resolution, hydrostatic solution of the outer domain and the high resolution, nonhydrostatic solution in the inner domain are particularly large at the western boundary. As the waves attempt to exit the inner domain this mismatch of solutions creates reflections which are very obvious in animations of the inner domain solutions of the experiments without the FRS.

One of the reflection events is shown using the temperature field at 150 m on the western side of the domain (Fig. 4). At hour 67 (Fig. 4A and A′) a NLIW front is clearly seen in the middle of the panel in both the FRS experiment (Fig. 4A′) and the experiment without FRS (Fig. 4A). Without the FRS the NLIW front approaches the western boundary and is reflected (Fig. 4A–D). The front is most obvious north of Dongsha Island. At hour 69 (Fig. 4B and B′) the front is approaching the western boundary. At hour 71 (Fig. 4C) it begins to intersect the western boundary and at hours 73 it can be seen reflecting from the western boundary and propagating back into the inner domain in the case without the FRS (Fig. 4D). The wave then travels back into the central region of the inner domain and significantly impacts the solution.

In the experiment with the FRS (Fig. 4A′ through D′) no part of the front is reflected from the western boundary. At hour 69 (Fig. 4B′), a wave front, similar to that seen in Fig. 4B, approaches the western boundary. At hour 71 (Fig. 4C′) it starts to intersect the western boundary. No reflected front is visible at hour 73 (Fig. 4D′). The solutions with the FRS and without the FRS are not identical. This is expected since there is less reflected energy in the FRS experiment than in the experiment without the FRS. Also, since the energy levels are different, the details of the solution in the inner domain will not be the same and the propagation speeds of the NLIWs and Submesoscale Features (SMFs) will also be different.

In addition to the qualitative visual assessment of the FRS, we have determined that the magnitude of $\overline{\overline{KE}}$ can be used as a quantitative measure. If NLIWs and SMFs are artificially reflected at the open boundaries then the magnitude of $\overline{\overline{KE}}$ should be larger in the inner domain. Values of $\overline{\overline{KE}}$ are listed in Table 2, where the largest $\overline{\overline{KE}}$ was found for the experiment with no FRS. This confirms our expectations that spurious reflections at the boundaries will lead to higher energy levels.

Experiments were then conducted to minimize $\overline{\overline{KE}}$ using the quadratic and hyperbolic tangent profiles, (9) and (10), and for

Table 2
Average kinetic energy in inner domain as a function of maximum relaxation coefficient and relaxation profile.

Relaxation profile	Maximum relaxation coefficient, $\sigma_m \times 10^2$	$\overline{KE}$ ($\times 100$)
No relaxation region	N/A	9.32
Quadratic	4	8.89
Hyperbolic tangent	4	8.80
Hyperbolic tangent	2	8.79
Hyperbolic tangent	1	8.78
Hyperbolic tangent	0.4	8.77
Hyperbolic tangent	0.2	8.78
Hyperbolic tangent	0.1	8.82
Hyperbolic tangent	0.02	8.93

several values of the maximum relaxation coefficient, σ_m. The results are shown in Table 2 and Fig. 5. From Table 2 it can be seen that in all FRS cases the $\overline{\overline{KE}}$ was lower than in the case with no FRS. The best results for the FRS are obtained with a small but finite σ_m and a hyperbolic tangent profile.

There does exist a σ_m which yields a minimum $\overline{\overline{KE}}$ as can be seen in Fig. 5 and Table 2. At one extreme σ_m cannot become arbitrarily small since as σ_m approaches zero the case with no FRS is recovered, see (10). However, neither can σ_m become arbitrarily large. This is a result of the discrete nature of the model. As σ_m becomes larger the spatial variation of the amplitude of the damped wave in the relaxation zone becomes too large to resolve with a given Δn. This is different from the continuous case where σ_m can become arbitrarily large since dn can be infinitesimal (MDD10).

The spatial variation of σ also matters. If σ changes too slowly across the relaxation zone the wave will not be completely damped before it passes through the relaxation zone and will be reflected off the outer domain edge of the relaxation zone. If σ changes too quickly the wave will be reflected near the inner domain edge of the relaxation zone. This is equivalent to moving the boundary close to the inner edge of the relaxation zone. A small correction which changes gradually at the interior edge of the relaxation zone and more rapidly as the outer domain is approached provides the best result. The hyperbolic tangent profile fits this criteria better than the quadratic profile. This is in agreement with the results of MDD10 and shows the importance of a spatially varying relaxation coefficient.

Although it is important to reduce or eliminate the reflection of NLIWs and other SMFs at the inner domain boundaries, it is also important to transmit information from the outer domain into the inner domain without altering the signals in either magnitude or phase. To check this we compare the inner domain solution to the outer domain solution cropped to the inner domain area (Fig. 6). The details of the two snapshots are different; however, the large scale patterns are very similar. This indicates that the information is being passed into the inner domain has maintained the low wavenumber characteristics of the outer domain solution.

To quantify this we compared wavenumber temperature spectra for the outer domain solution cropped to the inner domain area to that for the inner domain solution. First we took data along

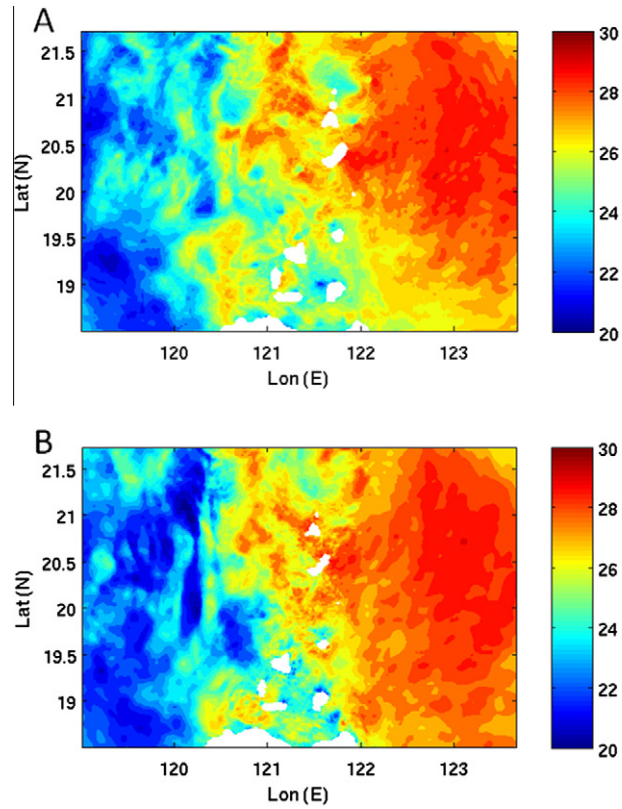

Fig. 6. (A) Temperature from inner domain solution and (B) outer domain solution cropped to inner domain area (bottom panel) at 95 m for hour 221.

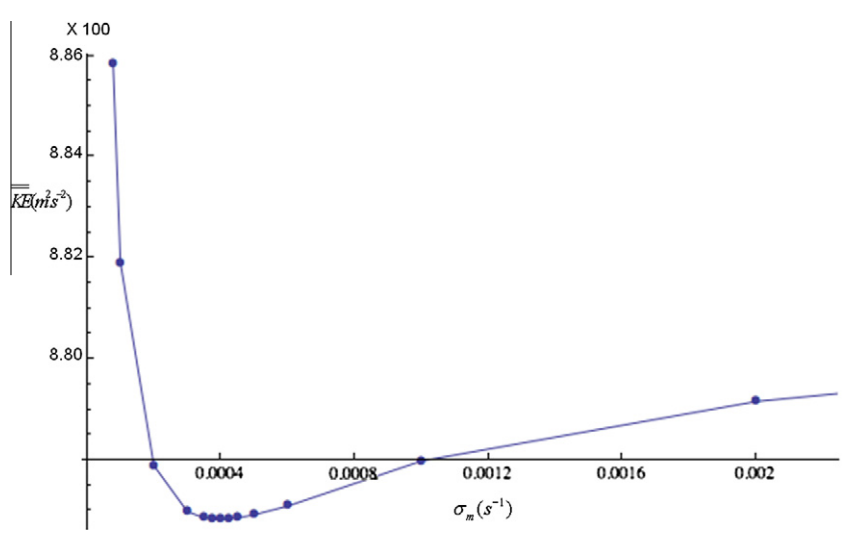

Fig. 5. Average horizontal kinetic energy ($\overline{\overline{KE}}$) as a function of the maximum absorption parameter (σ_m).

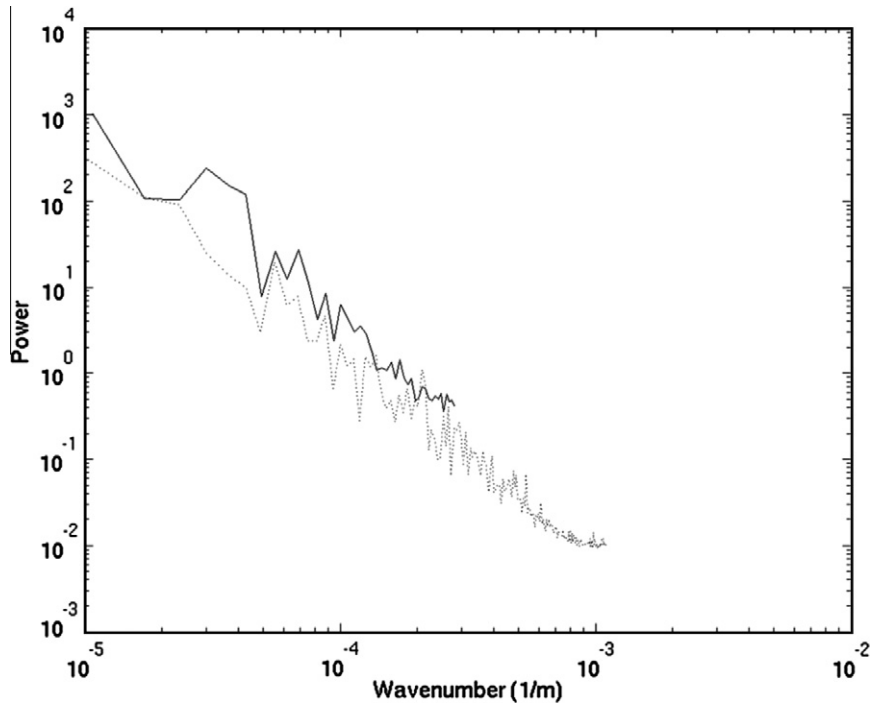

Fig. 7. Temperature spectra from the inner domain solution (dotted line) and the outer domain solution (solid line) cropped to the inner domain. Spectra were calculated along longitudes then averaged across latitudes.

longitudinal grid lines, using grid lines starting 10 grid points into the inner domain from the southern boundary and ending 10 grid points into the inner domain from the northern boundary. We calculated the spectrum along each of these lines then averaged the spectra over all lines. The resulting spectra are very similar up to the wavenumber cutoff for the outer domain (Fig. 7). The spectra from the inner domain continues to higher wavenumbers. This demonstrates that the low wavenumber energy has been passed from the outer domain solution to the inner domain solution with no appreciable alteration.

5. Conclusions

A nonhydrostatic model has been successfully embedded in a hydrostatic model as part of a prototype forecast/hindcast system. The key is a carefully crafted treatment of the prognostic variables near the open boundaries. Both a TCS, to conserve volume, and a FRS to merge the outer domain and inner domain solutions near the boundary are required for successful nesting. Hindcasts in the inner domain show high wavenumber, large amplitude features which are not present in the outer domain due to missing nonhydrostatic physics and resolution. The features in the inner domain agree with point observations. Obtaining area averaged time series data to verify $\overline{\eta_t^D}$ is a topic for future work. Verification of additional model data, e.g. T, S, u, v and w, with in situ and remotely sensed data are in progress and will be reported in another paper.

Domains must be nested Matryoshka (Russian Doll) style to achieve the resolution needed to model submesoscale dynamics as part of a global system. To accomplish realistic hindcasts the submesoscale domain must be nested in a mesoscale domain, which is nested in a regional domain, which is nested inside a global domain. Through the combination of real-time forecast systems and off-line hindcast systems we can achieve a global to submesoscale modeling system.

Open boundaries naturally occur when modeling submesoscale dynamics since the domains of interest are limited by the small grid spacing needed to resolve the dynamics. The boundaries must provide information about the larger scale outer domain dynamics on the inner domain grid without introducing erroneous trends. Also the mismatches of the solutions in the inner and outer domains must be adjusted at the boundaries to prevent contamination of the inner domain solution. These mismatches, caused by differences in resolution, physics and numerics, manifest at the boundaries of the inner domain as reflections of momentum and energy and as spurious perimeter currents.

OBCs from the outer domain must be mapped onto the inner domain grid and must be adjusted to conserve volume. We used a TCS to adjust the baroclinic normal velocities such that the change in η is balanced by the total barotropic transport through the open boundaries. The baroclinic normal velocities are weighted by the lateral surface area of the grid cell adjacent to the open boundaries to conserve total transport. This method improves model performance. Techniques for improving this method and gathering observations for comparison are topics of ongoing and future work.

Dynamic features generated or transformed in the inner domain can be quite different from those in the outer domain. In fact some dynamic features in the inner domain will not be present in the outer domain. This can be due to increased resolution in the inner domain, in which case the features are not resolved in the outer domain. It can be due to differences in hydrostatic versus nonhydrostatic physics, in which case the feature would not exist in the outer domain even if the resolution in the two domains was the same. Finally this can be due to differences in the numerics or the numerical parameters between the two domains, in which case the features might be damped out or dissipated in the outer domain. In any case the differences will be manifested as discrepancies in the prognostic variables near the open boundaries. This can lead to reflections, perimeter currents and other spurious features of the solution on the inner domain. These spurious features

cannot be allowed to propagate into the inner domain and contaminate the results. A solution is to construct a relaxation zone along the perimeter of the inner domain where these spurious features are removed from the inner domain solution using a FRS.

It is desirable to have the relaxation zone as narrow as possible to maximize the area available for the inner domain solution. At the same time the spurious features must be damped well enough that they do not significantly impact the solution in the inner domain or the boundary values from the outer domain. The spatial characteristics and maximum value of relaxation coefficient are both important to the effectiveness of FRS in the relaxation zone. We have shown that a relatively small relaxation coefficient with a hyperbolic tangent spatial distribution that varies slowly near the inner domain side of the relaxation zone and varies rapidly near the outer domain side of the relaxation zone yields the best results. This is in agreement with previous findings by other authors.

Nonhydrostatic physics is required to obtain the correct dynamics for the submesoscale domain. This increases the differences between the inner domain and outer domain solutions which complicates the task of reconciling the two solutions near the boundaries. This necessitated a careful treatment of both the TCS and the FRS.

Acknowledgements

This research was supported by the ONR Internal Waves in Straits Experiment DRI (IWISE – N0001409WX20632), the ONR Philippines Straits Experiment (PhilEx) DRI (N0001411AF00002) and the ONR NonLinear Waves Initiative (NLIWI) DRI (N0001408WX20931). The numerical experiments were conducted at the NAVY DoD Supercomputer Resource Center (DSRC) and the ERDC DSRC and were supported by the High Performance Computing Modernization Program (HPCMP) project Nonhydrostatic Ocean Modeling (NRLSS30275065).

We wish to thank Dr. Dong Shan Ko for providing the data from the LZS64 NCOM hindcasts and Ms. Shelley Riedlinger for providing the data from the EAS16NFS forecasts. We also wish to thank two anonymous reviewers for comments which significantly improved the manuscript.

References

Accadia, C., Mariani, S., Casaioli, M., Lavagnini, A., Speranza, A., 2003. Sensitivity of precipitation forecast skill scores to bilinear interpolation and a simple nearest-neighbor average method on high-resolution verification grids. Weather Forecast. 18, 918–932.

Adcroft, A., Hill, C., Marshall, J., 1997. Representation of topography by shaved cells in a height coordinate ocean model. Mon. Weather Rev., 2293–2315.

Barron, C.N., Kara, A.B., Martin, P.J., Rhodes, R.C., Smedstad, L.F., 2006. Formulation, implementation and examination of vertical coordinate choices in the Global Navy Coastal Ocean Model (NCOM). Ocean Modell. 11, 347–375.

Beardsley, R., Duda, T., Lynch, J., Irish, J., Ramp, S., Chiu, C., Tang, T., Yang, Y., Fang, G., 2004. Barotropic tide in the northeast South China Sea. IEEE J. Ocean. Eng. 29, 1075–1086.

Blayo, E., Debreu, L., 2005. Revisiting open boundary conditions from the point of view of characteristic variables. Ocean Modell. 9, 231–252.

Chao, S.Y., Ko, D.S., Lien, R.C., Shaw, P.T., 2007. Assessing the west ridge of luzon strait as an internal wave mediator. J. Oceanogr. 63, 897–911.

Coelho, E., Peggion, G., Rowley, C., Jacobs, G., Allard, R., Rodriguez, E., 2009. A note on NCOM temperature forecast error calibration using the ensemble transform. J. Marine Syst. 78, S272–S281.

Davies, H.C., 1983. Limitations of some common lateral boundary schemes used in regional NWP models. Mon. Weather Rev. 111, 1002–1012.

Egbert, G.D., Bennett, A.F., Foreman, M.G.G., 1994. Topex/Poseidon tides estimated using a global inverse model. J. Geophys. Res. Ocean. 99, 24821–24852.

Flather, B.A., 1976. A tidal model of the northwest European continental shelf. Mem. Soc. R. Sci. 6, 24.

Guo, X.Y., Hukuda, H., Miyazawa, Y., Yamagata, T., 2003. A triply nested ocean model for simulating the Kuroshio – Roles of horizontal resolution on JEBAR. J. Phys. Oceanogr. 33, 146–169.

Hodur, R.M., 1997. The Naval Research Laboratory's coupled ocean/atmosphere mesoscale prediction system (COAMPS). Mon. Weather Rev. 125, 1414–1430.

Hogan, T.F., Rosmond, T.E., 1991. The description of the navy operational global atmospheric prediction systems spectral forecast model. Mon. Weather Rev. 119, 1786–1815.

Jan, S., Chern, C., Wang, J., Chao, S., 2007. Generation of diurnal $K-1$ internal tide in the Luzon Strait and its influence on surface tide in the South China Sea. J. Geophys. Res. Ocean. 112.

Jensen, T., 1998. Open boundary conditions in stratified ocean models. J. Marine Syst., 297–322.

Lavelle, J.W., Thacker, W.C., 2008. A pretty good sponge: Dealing with open boundaries in limited-area ocean models. Ocean Modell. 20, 270–292.

Lien, R.C., Tang, T.Y., Chang, M.H., D'Asaro, E.A., 2005. Energy of nonlinear internal waves in the South China Sea. Geophys. Res. Lett., 32.

Marchesiello, P., 2001. Open boundary conditions for long-term integration of regional ocean models. Ocean Modell. 3, 1–20.

Marshall, J., Adcroft, A., Hill, C., Perelman, L., Heisey, C., 1997a. A finite-volume, incompressible Navier Stokes model for studies of the ocean on parallel computers. J. Geophys. Res. Ocean. 102, 5753–5766.

Marshall, J., Hill, C., Perelman, L., Adcroft, A., 1997b. Hydrostatic, quasi-hydrostatic, and nonhydrostatic ocean modeling. J. Geophys. Res. Ocean. 102, 5733–5752.

Martinsen, E.A., Engedahl, H., 1987. Implementation and testing of a lateral boundary scheme as an open boundary-condition in a barotropic ocean model. Coastal Eng. 11, 603–627.

Mason, E., Molemaker, J., Shchepetkin, A.F., Colas, F., McWilliams, J.C., Sangra, P., 2010. Procedures for offline grid nesting in regional ocean models. Ocean Modell. 35, 1–15.

Modave, A., Deleersnijder, E., Delhez, E.J.M., 2010. On the parameters of absorbing layers for shallow water models. Ocean Dyn. 60, 65–79.

Orlanski, I., 1976. Simple boundary-condition for unbounded hyperbolic flows. J. Comput. Phys., 251–269.

Palma, E., Matano, R., 1998. On the implementation of passive open boundary conditions for a general circulation model: The barotropic mode. J. Geophys. Res. Ocean., 1319–1341.

Riedlinger, S., Preller, R., Martin, P. 2006. Validation test report for the east Asian seas navy coastal ocean model nowcast/forecast system, In: Laboratory, N.R. (Ed.).

Shulman, I., Wu, C.R., Lewis, J.K., Paduan, J.D., Rosenfeld, L.K., Kindle, J.C., Ramp, S.R., Collins, C.A., 2002. High resolution modeling and data assimilation in the Monterey Bay area. Cont. Shelf Res. 22, 1129–1151.